

## REVIEW ARTICLE

DOI: 10.1038/s41467-018-04866-6

OPEN

# Two-dimensional semiconductors in the regime of strong light-matter coupling

Christian Schneider<sup>1</sup>, Mikhail M. Glazov<sup>2</sup>, Tobias Korn<sup>3</sup>, Sven Höfling<sup>1,4</sup> & Bernhard Urbaszek<sup>5</sup>

The optical properties of transition metal dichalcogenide monolayers are widely dominated by excitons, Coulomb-bound electron–hole pairs. These quasi-particles exhibit giant oscillator strength and give rise to narrow-band, well-pronounced optical transitions, which can be brought into resonance with electromagnetic fields in microcavities and plasmonic nanostructures. Due to the atomic thinness and robustness of the monolayers, their integration in van der Waals heterostructures provides unique opportunities for engineering strong light-matter coupling. We review first results in this emerging field and outline future opportunities and challenges.

**T**ransition metal dichalcogenides (TMDCs) are ideally suited as the active material in cavity quantum electrodynamics, as they interact strongly with light at the ultimate monolayer limit. They exhibit pronounced exciton resonances even at room temperature owing to the exceptionally high exciton binding energies of a few 100 meV<sup>1,2</sup>.

The high exciton oscillator strength leads to absorption of up to 20% per monolayer<sup>3</sup>, and radiative exciton lifetimes on the order of few 100 fs to several ps<sup>4–7</sup>. In TMDC monolayers (MLs), the dipole selection rules are valley-selective, i.e., distinct valleys in momentum space can be addressed by photons with left- or right-handed helicity<sup>8–12</sup>. In combination with strong spin–orbit splitting, this allows studying intertwined spin-valley dynamics of excitons<sup>13–15</sup>. These unique optical properties make monolayer TMDCs, which can readily be embedded in the van der Waals heterostructures containing multiple active layers<sup>16,17</sup>, ideal systems for investigating excitons, and their interactions with other electromagnetic excitations.

This review paper is structured as follows. First, we provide a concise description of the optical properties of excitons in TMDC MLs. We then present the generic concept of strong light-matter coupling which arises for excitons confined in the TMDC monolayer interacting with photons trapped inside a cavity or plasmons localized in a metallic nanosystem. Strong light-matter coupling gives rise to half-light–half-matter quasi-particles, which are also known as exciton-polaritons<sup>18–20</sup>. This generally results in a substantial modification of the emission properties yielding an oscillatory behavior between light- and matter excitations in the temporal, and the emergence of the characteristic Rabi splitting in the spectral domain, for comparison with light-matter coupling in conventional semiconductors see Box 1 and refs. <sup>21,22</sup>. We review recent experimental advances of strong light-matter coupling in TMDC MLs and discuss complementary system implementations which were designed to study the formation of exciton-polaritons with atomic MLs.

<sup>1</sup>Technische Physik and Wilhelm Conrad Röntgen Research Center for Complex Material Systems, Physikalisches Institut, Universität Würzburg, Am Hubland, 97074 Würzburg, Germany. <sup>2</sup>Ioffe Institute, St. Petersburg, Russia 194021. <sup>3</sup>Institut für Experimentelle und Angewandte Physik, Universität Regensburg, 93040 Regensburg, Germany. <sup>4</sup>SUPA, School of Physics and Astronomy, University of St. Andrews, St. Andrews, KY 16 9SS, UK. <sup>5</sup>Université de Toulouse, INSA-CNRS-UPS, LPCNO, 135 Avenue de Rangueil, 31077 Toulouse, France. Correspondence and requests for materials should be addressed to B.U. (email: [urbaszek@insa-toulouse.fr](mailto:urbaszek@insa-toulouse.fr))

**Box 1 | Exciton-polaritons in cavity structures with atomic monolayers vs. conventional quasi-two-dimensional semiconductors**

A field of exciton-polariton physics is an important discipline of solid-state cavity quantum electronics, which relies on strong light-matter coupling in microcavities. Exciton-polaritons, or, in short, polaritons emerge in high quality microcavities with embedded active material comprising a sufficiently large exciton oscillator strength, and a sufficiently small mode volume (conditions for strong coupling are detailed in the main text). Cavity exciton-polaritons have first been observed in a GaAs-quantum well microcavity where a quasi-two-dimensional quantum well served as an active medium, and ever since, this material platform has remained the workhorse implementation to study linear, non-linear and collective polaritonic effects. By now exciton-polaritons have been observed in photonic structures hosting a large variety of active materials. Apart from GaAs, extensive investigations have been carried out to study polaritons in GaN, ZnO and other II-VI-based structures, organic polymers, carbon nanotubes, and more recently TMDC monolayers. Key prerequisites for an ideal material system in polariton research involve:

**Large exciton binding energy:** The limitation in exciton binding energies in most III-V materials set an upper temperature and density limit to the presence of the polariton condensate phase, which significantly limits their applicability to cryogenic temperatures. With the exception of GaN- and ZnO-based structures, which, however, frequently suffer from severe issues related to electrical injection in DBR structures, organic materials have moved to the focus, supporting the formation of polariton condensates at room-temperature. However, it remains very challenging to overcome strong excitonic localization and the notorious bleaching effects in organic materials in the near future. TMDC polaritons certainly have a potential to outperform most materials in this regard, thanks to their enormous binding energies and giant oscillator strength.

**Electrical injection** is highly desirable for any practical optoelectronic device. While electrically injected polariton condensation in GaAs microcavities has been addressed in the past, a realization of a high quality, microcavity-based room-temperature prototype will still constitute a major breakthrough in the field. Unlike most traditional material platforms for high temperature polaritonics, current injection into atomic monolayers is proven feasible.

**Low disorder:** Exciton localization and disorder represent a major obstacle for the generation of clean, spatially nonfragmented condensates and polariton devices relying on a rapid expansion of coherent states, such as polariton circuits. Thus far, GaAs represents the sole material platform where effects of macroscopic expansion and propagation of polaritonic condensates are reliably observed. With the recent development on reduced excitonic disorder in encapsulated monolayers, TMDC polaritons have the potential to become a serious competitor.

**Spin Textures:** The polariton system is a prime candidate to study spin-physics in coherent condensates. However, those studies have been restricted to polaritons in GaAs-based structure. TMDC monolayers benefit from having, in addition to the spin degree of freedom, the valley degree of freedom. It opens up a new field of spin and valley physics in cavity electrodynamics.

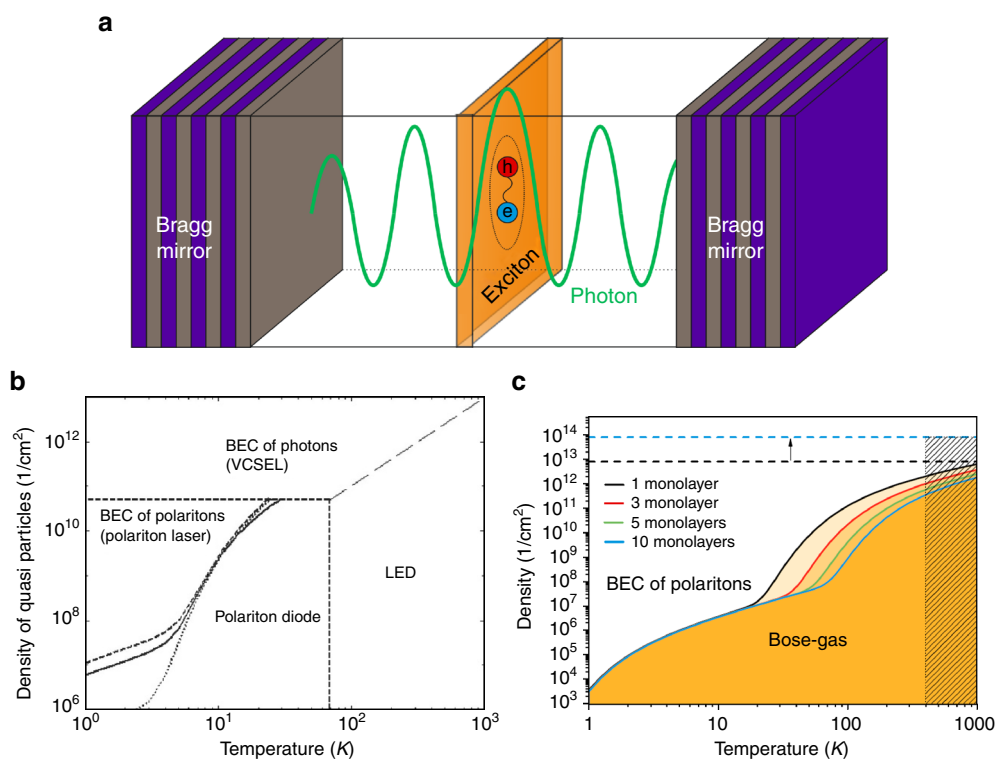


**Fig. 1.** (a) schematics of a microcavity with embedded active media supporting excitons. (b) phase diagrams of equilibrium exciton-polaritons in conventional GaAs-based structure from Ref. [21], adapted from Kavokin et al, 2003. © 2003 Materials Research Society (c) phase diagrams of equilibrium exciton-polaritons in the structure containing TMDC monolayers from Ref. [22]. BEC is Bose-Einstein condensate. reproduced from Lundt, N et al, Monolayered MoSe<sub>2</sub>: a candidate for room temperature polaritonics, 2D Materials Volume 4, Number 1, 2016. Published under a Creative Commons CC BY 3.0 license

**Excitonic and optical properties of TMDC MLs**

Semiconducting TMDCs are part of the large group of layered materials widely investigated for fundamental research and applications following the discovery of graphene<sup>23</sup>. The remarkably simple mechanical exfoliation techniques give access to rather large-area monolayer samples. While exfoliation of TMDC

MLs was already demonstrated in a seminal work by Novoselov et al.<sup>24</sup> in 2005, the observation of pronounced photoluminescence in MoS<sub>2</sub> MLs, reported by two groups<sup>25,26</sup> in 2010, triggered intense research activities regarding the optical and electronic properties of atomically thin TMDCs. MLs of MoS<sub>2</sub> and related TMDCs consist of a hexagonally coordinated

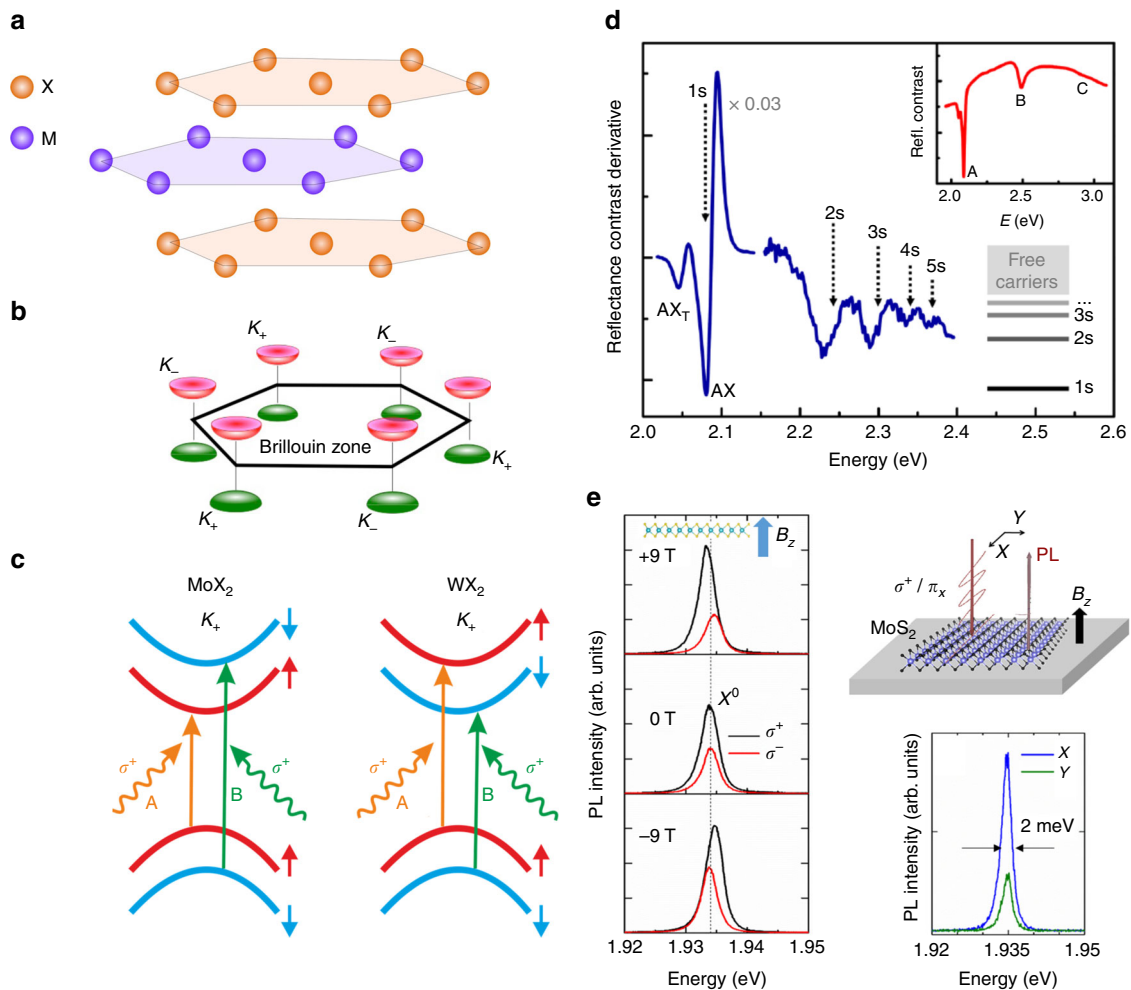


**Fig. 1** Crystal and band structure of semiconducting TMDCs. **a** Schematic view of TMDC monolayer crystal structure. **b** Band structure of TMDC monolayer with direct optical band gap at  $K$  points. **c** Valley-specific selection rules for molybdenum-based ( $\text{MoX}_2$ ) and tungsten-based ( $\text{WX}_2$ ) compounds. **d** Evolution of exciton states for  $\text{WS}_2$  monolayer on  $\text{SiO}_2$ <sup>2</sup>, reproduced from Chernikov et al.<sup>2</sup> © American Physical Society. **e** Optical valley initialization and valley coherence generation for a  $\text{MoS}_2$  monolayer encapsulated in  $\text{hBN}$ <sup>45</sup> reproduced from Cadiz et al.<sup>45</sup>

transition metal atom layer sandwiched between top and bottom chalcogen layers, which are also hexagonally coordinated, leading to a trigonal prismatic crystal structure<sup>27,28</sup> (see Fig. 1a) described by the  $D_{3h}$  point symmetry group. Correspondingly, the monolayer does not have inversion symmetry. The bulk TMDC crystal is formed by van der-Waals-mediated stacking the monolayer units. In the 2H stacking sequence, which is the most prevalent polytype, inversion symmetry is recovered for even numbers of layers and eventually in the bulk crystal.

Bulk  $\text{MoS}_2$  is an indirect-gap semiconductor with a valence band maximum at the  $\Gamma$  point, the center of its hexagonal Brillouin zone, and conduction-band minima located in between the  $\Gamma$  and the  $K$  points at the corners of the Brillouin zone. In the monolayer limit, however, the character of the band-gap changes to a direct gap at the  $K$  points (see Fig. 1b)<sup>25,26,29,30</sup>. A similar transition of the band structure from indirect to direct also occurs in the related TMDCs  $\text{WS}_2$ ,  $\text{MoSe}_2$ ,  $\text{WSe}_2$ ,  $\text{MoTe}_2$ , and their alloys. In the TMDC MLs, the band structure at the  $K$  valleys is characterized by a very large, valley-contrasting spin splitting in the valence bands, whose magnitude ranges from about 150 meV ( $\text{MoS}_2$ ) to more than 450 meV ( $\text{WSe}_2$ ), and a smaller, yet still substantial spin splitting in the conduction band<sup>31–33</sup>. As the optical transitions between the valence and conduction band are spin-conserving, this splitting gives rise to two, spectrally well-

separated interband optical transitions identified as A (transition from the upper valence band) and B (transition from the lower valence band), see Fig. 1c.

The optical properties of TMDCs are determined by the formation of tightly bound exciton states, which have binding energies on the order of several hundred meVs<sup>1,2,34,35</sup>, making them stable well beyond room temperature. The large binding energies arise due to a combination of several effects: electrons and holes at the  $K$  points of the Brillouin zone have rather large effective masses (ranging from about  $0.25 m_e$  to  $0.6 m_e$  depending on the specific TMDC<sup>35</sup> where  $m_e$  is the free-electron mass) and are strictly confined to the two-dimensional plane of the monolayer. Additionally, their Coulomb interaction is only weakly screened, and this screening typically is anisotropic due to the anisotropic dielectric environment<sup>36,37</sup>. This leads to a strong deviation of excited exciton state energies from a hydrogen-like Rydberg series, illustrated in Fig. 1d<sup>1,2</sup>. It is worth noting, that engineering the dielectric environment of the monolayer, e.g., by encapsulating the TMDC between other layered materials, or modifying the substrate, allow for a controlled tuning both of the band gap and the exciton binding energy<sup>38,39</sup>. The large radiative decay rate of excitons  $\Gamma_0 \gtrsim 1 \text{ ps}^{-1}$  and, correspondingly, high oscillator strength  $f = \Gamma_0/\omega_0 \gtrsim 10^{-3}$ , with  $\omega_0$  being the exciton resonance frequency, results in efficient light-matter interactions

in TMDC MLs. The exact values of  $f$  and  $\Gamma_0$  will also depend on the dielectric environment<sup>4–7,40,41</sup>. The short radiative lifetime yields a significant homogeneous spectral broadening of the excitonic transitions<sup>42</sup>. It also leads to a large coupling constant  $g$  with photonic modes in microcavity structures, as detailed below<sup>43</sup>. The high oscillator strength of the excitonic transitions gives rise to a very large absorption for the A-exciton transition in the tungsten-based TMDCs<sup>1,44</sup>. Theoretically, the maximal absorbance of a monolayer  $A_{\max}$  at resonance is controlled by the ratio of the radiative to the non-radiative,  $\gamma$ , decay rate of the excitons,  $A_{\max} = 2I_0/(\Gamma_0 + \gamma)^2$  and may reach 50% under optimal conditions of  $\Gamma_0 = \gamma$ . While the emission from typical TMDC samples deposited on SiO<sub>2</sub> is strongly inhomogeneously broadened by adsorbates and substrate-induced effects, recent advances in sample fabrication (encapsulation in hexagonal BN) yield linewidths indeed approaching the homogeneous limit, see Fig. 1e<sup>45–47</sup>.

The transition metal atoms of the TMDCs strongly influence not only the magnitude of the spin splitting, but also the ordering of the spin-split conduction bands (see Fig. 1c). While for MoX<sub>2</sub>, the optically bright A-exciton transition connects the upper valence band with the lower conduction band, the band order is opposite in the tungsten-based materials, so that the A-exciton transition addresses the upper conduction band<sup>33,48</sup>. Thus, for WX<sub>2</sub> MLs, the exciton state lowest in energy with the electron residing in the lower spin-split conduction band is forbidden in optical transitions for normal light incidence. The splitting between the optically bright and dark states is given by a combination of the conduction-band spin splitting and electron–hole Coulomb exchange interaction<sup>49</sup>. The lower-energy dark A-exciton state in the tungsten-based materials was indirectly inferred from temperature-dependent PL measurements<sup>50–52</sup>. More recently, PL emission from the dark state was directly observed using applied in-plane magnetic fields<sup>53,54</sup> and in-plane excitation and detection geometry<sup>55–57</sup>. In addition to neutral excitons, charged excitons (trions)<sup>58</sup> with binding energies of about 25 meV are observable in optical spectroscopy, and the multi-valley band structure allows for different trion species<sup>13,59–61</sup>. Four-particle complexes, biexcitons, i.e., excitonic molecules have also been observed<sup>62–64</sup>.

The optical selection rules for interband transitions<sup>9</sup> allow for valley-selective excitation at the  $K^+$  or  $K^-$  valleys using  $\sigma^+$  or  $\sigma^-$ -polarized light, respectively. Thus, near-resonant, circularly polarized excitation generates a valley polarization of excitons, which can be read out directly in helicity-resolved photoluminescence. Even in time-integrated (cw) photoluminescence measurements, large valley polarization degrees are observable for most TMDC MLs<sup>8–12,65</sup>. These initial observations motivate the use of the valley pseudospin in potential device applications (valleytronics)<sup>66</sup>. However, the large cw valley polarization values are, in part, a consequence of the ultrashort exciton radiative lifetime limiting the time window for valley polarization decay. The dominant decay mechanism for excitonic valley polarization is long-range electron–hole exchange interaction<sup>67,68</sup>. Its efficiency scales with the exciton center-of-mass momentum and the resulting decay rate can rival the exciton radiative lifetime, dependant on excitation conditions. In contrast, valley polarization lifetimes are orders of magnitude longer for dark excitons<sup>13,69</sup>, interlayer excitons in TMDC heterostructures<sup>70</sup> and resident carriers in doped TMDC MLs<sup>15,71</sup>.

### General framework of strong light-matter coupling

An optically active exciton in an isolated TMDC ML emits photons into the free space. In addition to the symmetry-imposed

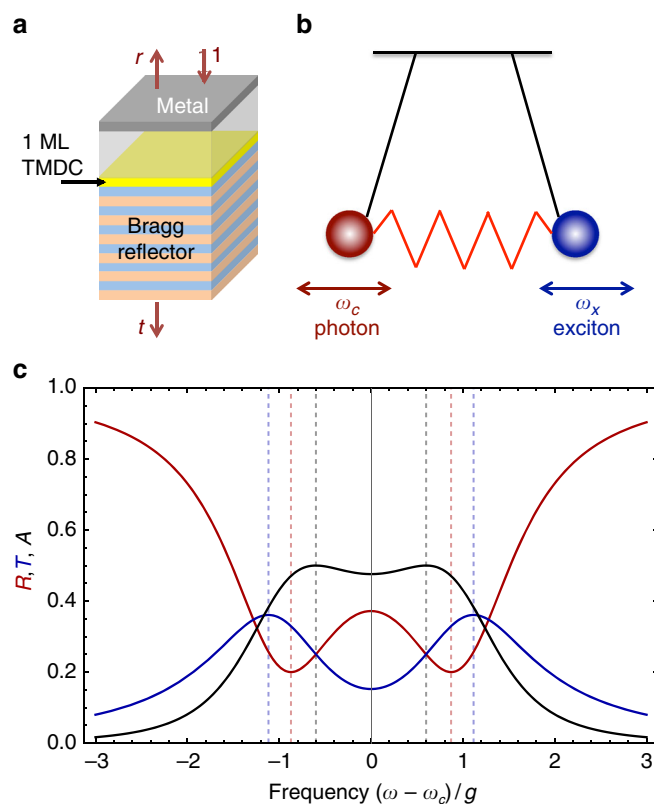


**Fig. 2** Basic concept of strong coupling. **a** Sketch of the TMDC ML in an optical microcavity fabricated using a distributed Bragg reflector (bottom layers) and a metallic layer on top. **b** Illustration of the coupled-oscillators model describing the coherent energy transfer between the cavity photon and exciton. **c** Reflection ( $R = |r|^2$ , red curve), transmission ( $T = |t|^2$ , blue curve) and absorption ( $A = 1 - R - T$ , black curve) coefficients calculated for the structure in **a** for the strong-coupling parameters  $\omega_c = \omega_x$  and  $\kappa = \gamma = 0.8g$

valley selection rules described above, the photon emission process obeys energy and momentum conservation laws, making only excitons with small in-plane wavevectors,  $|K| < \omega_x/c$ , i.e., within the light cone, subject to the radiative processes. Here,  $c$  is the speed of light and  $\omega_x$  is the exciton resonance frequency, largely determined by the difference between the free carrier band gap and the exciton binding energy. As emitted light propagates away from the ML carrying away the energy<sup>67,72</sup>, the exciton experiences radiative damping. Note that excitons with  $|K| > \omega_x/c$  are optically inactive and can contribute to the PL only after relaxation towards the radiative cone. The situation becomes qualitatively different if the emitted light cannot leave the vicinity of the ML, e.g., if the ML is placed between two mirrors which form an optical cavity, Fig. 2a, or if a ML is placed in the vicinity of a metallic or dielectric nanoparticle supporting plasmonic or Mie resonances. In such situations, the exciton effectively interacts with a localized mode of electromagnetic radiation (or a plasmon) with the frequency  $\omega_c$ . Hence, the emitted photon can be reabsorbed by the TMDC ML and reemitted again. This emission-absorption process repeats until either the exciton in the ML vanishes due to scattering or non-radiative processes or the photon leaves the cavity, e.g., as a result of the tunneling through the mirrors. If these decay processes are weak enough the excitation energy is coherently transferred between the exciton and the photon (or plasmon) resulting in the strong-coupling regime of the light-matter interaction and giving rise to a qualitative



change of the energy spectrum in the system: instead of independent exciton and photon states new eigenmodes of the system, the exciton-polaritons, are formed<sup>18,19</sup>.

There are several approaches to describe theoretically the strong-coupling effects. It is instructive to consider here the coupled-oscillators model where the excitonic contribution to the dielectric polarization in the TMDC ML,  $\mathbf{P}$ , and the electric field of the cavity mode,  $\mathbf{E}$ , are treated on a semi-classical level and are assumed to obey the oscillator like equations of motion:

$$i\dot{\mathbf{P}} = (\omega_x - i\gamma)\mathbf{P} + g\mathbf{E}, \quad (1)$$

$$i\dot{\mathbf{E}} = (\omega_c - i\kappa)\mathbf{E} + g\mathbf{P}. \quad (2)$$

Here, a dot on top denotes the time derivative,  $\gamma$  and  $\kappa$  are the dampings, respectively, of the exciton and cavity mode unrelated to the light-matter coupling (which determine half-width at half maximum of the resonances), and  $g$  is the coupling constant which is determined by the system geometry and exciton oscillator strength. For a planar microcavity, it can be roughly estimated as  $g \sim \sqrt{\omega_c \Gamma_0}$ , where the proportionality constant depends on the cavity geometry and structure of the Bragg mirrors,  $\Gamma_0$  is the exciton radiative decay rate into empty space. Here the large exciton oscillator strength resulting in large  $\Gamma_0$  allowing to estimate values of  $\hbar g \sim 10 \dots 50$  meV depending on the system parameters. These high values for  $g$  present one of the intrinsic advantages for studying light-matter coupling in TMDC MLs as compared to nanostructures with transitions with lower oscillator strength. Equation (1) can be formally derived from Maxwell equations for the electromagnetic field in the cavity and the Schrödinger equation for the exciton wavefunction in the resonant approximation assuming that  $\gamma, \kappa, g \ll \omega_x, \omega_c$ <sup>41</sup>. It follows from Eq. (1) that for the harmonic time-dependence of the polarization and field  $\mathbf{P}, \mathbf{E} \propto e^{-i\omega t}$  the eigenfrequency  $\omega$  can be found from the simple quadratic equation:

$$(\omega - \omega_x + i\gamma)(\omega - \omega_c + i\kappa) = g^2, \quad (3)$$

which indeed describes eigenfrequencies of two damped oscillators coupled with the constant  $g$ . Equation (3) can be also derived from the transfer matrix method, which describes propagation of electromagnetic waves in a planar structure or by the procedure of the excitonic and electromagnetic field quantization<sup>41,43,73,74</sup>.

The general solution of Eq. (3) is found in many references, e.g.,<sup>19,41,75</sup>, here we consider the simplest but already instructive case at resonance  $\omega_x = \omega_c \equiv \omega_0$ , which already allows one to identify the strong and weak-coupling regimes. In this case the solutions of Eq. (3) read

$$\omega_{\pm} = \omega_0 - i \frac{\gamma + \kappa}{2} \pm \frac{\Omega_R}{2}, \quad \Omega_R = \sqrt{4g^2 - (\gamma - \kappa)^2}. \quad (4)$$

Here  $\Omega_R$  is the Rabi frequency related to the so-called vacuum-Rabi splitting,  $\hbar\Omega_R$ , of polariton modes in quantum electrodynamics. In the strong-coupling regime the Rabi frequency is real, i.e.,

$$\text{Strong coupling : } g > |\gamma - \kappa|/2, \quad (5)$$

In contrast, for  $g < |\gamma - \kappa|/2$  the light-matter interaction is in the weak-coupling regime. The strong coupling means that the real parts of the eigenfrequencies are split by  $\Omega_R$ , while their imaginary parts responsible for the damping are equalized. In the weak coupling, by contrast, the light-matter coupling affects the damping rates giving rise to the Purcell-like enhancement of suppression of the exciton radiative decay<sup>76,77</sup>. Hence, in the strong-coupling regime an anticrossing between the photon and exciton modes should be observed, while in the weak coupling the

photon and exciton modes in optical spectra cross each other at the variation of the cavity resonance  $\omega_c$  (e.g., via the incidence angle) or the exciton resonance  $\omega_x$  (e.g., via the sample temperature).

Equation (5) provides a formal criterion of the strong-coupling regime. In realistic systems, however, the damping of polariton modes  $(\gamma + \kappa)/2$  can be comparable to  $\Omega_R$ , making identification of the Rabi splitting difficult. Moreover, the splitting of peaks in different experiments has different amplitudes<sup>43</sup>: In Fig. 2c, we compare the cavity reflection coefficient  $R$ , transmission coefficient,  $T$ , and absorbance  $A = 1 - R - T$  for  $\gamma, \kappa \lesssim \Omega_R$  where these quantities are found within the input-output formalism<sup>74</sup>. Therefore different experiments, also including PL, on the same sample will give different splittings due to strong coupling that are not directly the Rabi splitting, but are related to it, as detailed in ref. <sup>43</sup>

The model discussion above disregards the nonlinear effects related with the exciton-exciton interactions and the oscillator strength saturation. Since excitons are tightly bound in TMDC MLs, these effects are somewhat weaker compared with conventional semiconductor quantum wells, particularly, the exciton oscillator strength saturation is controlled by the parameter  $n_{\text{exc}} a_B^2$ , where  $n_{\text{exc}}$  is the exciton density and  $a_B$  is the Bohr radius.

### Strong coupling in nanostructures with semiconducting 2D active layers

**Strong coupling of MLs in all-dielectric microcavities.** As described above, the combination of high exciton binding energies, large oscillator strength and the possibility to strongly reduce structural disorder naturally puts sheets of TMDCs in the focus of polaritonic research. In most III-V, and specifically GaAs-based implementations of polaritonic devices, the cavity design of choice is a high-quality-factor Fabry-Perot resonator based on highly reflecting distributed Bragg reflectors (DBRs), which sandwich the active layer. While, in principle, the transfer of a single, or multiple TMDC layers on top of a DBR mirror is straight forward, optimal methods to sandwich layers in high-Q DBR-resonators are currently still being developed. This task is closely related to designing and integrating high-quality van der Waals heterostructures (such as MLs encapsulated by hBN layers), which reduce inhomogeneous and non-radiative broadening effects dramatically, in more complex devices. Nevertheless, in a first experimental effort, signatures of the strong-coupling regime have been found in a device featuring a single flake of MoS<sub>2</sub>, synthesized via chemical vapor deposition, that was embedded in a dielectric DBR cavity<sup>78</sup>. There, the authors studied both the reflection spectra as well as the photoluminescence as a function of the in-plane momentum at room temperature. While in this initial experiment, the anticrossing of the normal modes could not be fully mapped out, various groups later on implemented new generations of devices to scrutinize the coupling conditions between confined light-fields and monolayer excitons: a clear cut proof of strong-coupling conditions at cryogenic temperatures has been reported by Dufferwiel et al.<sup>79</sup>, for the case of single and double layers of MoSe<sub>2</sub>, which were embedded in a so-called open cavity based on two separated DBR mirrors, see Fig. 3a and b. In this work, the authors established the formation of exciton-polaritons by fully mapping out the anticrossing of the two resonances in a cavity detuning experiment. A similar implementation, based on an open fiber cavity was reported more recently in ref. <sup>80</sup>, where strong-coupling conditions were manifested in charge-tunable studies both at the characteristic exciton as well as the trion resonance energies, and the results were interpreted in the framework of coupling to attractive and repulsive polaron resonances. For a monolayer of WS<sub>2</sub>, the

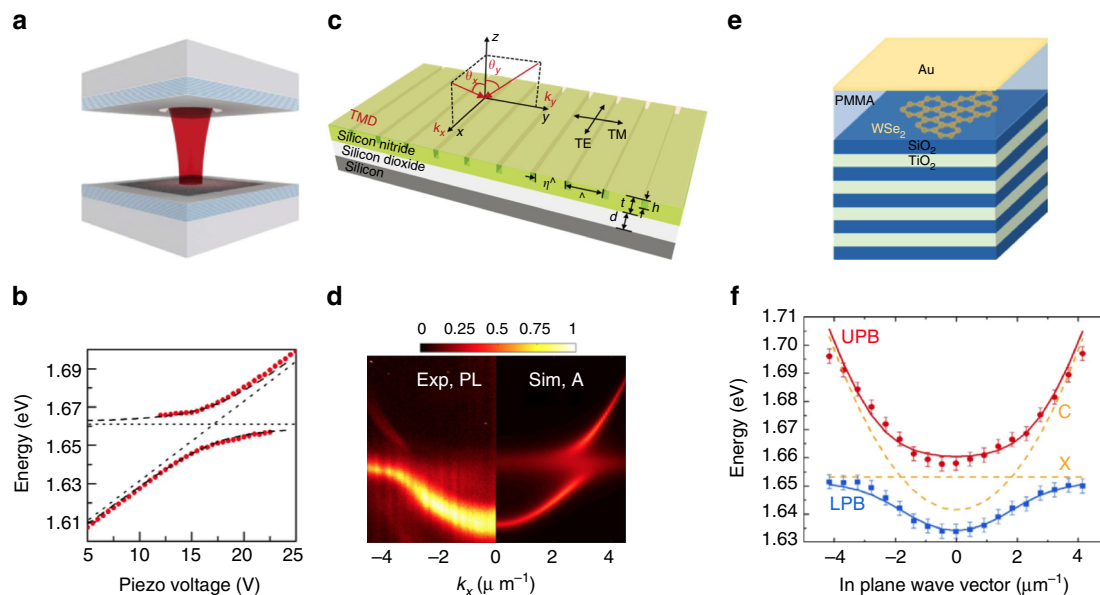


**Fig. 3** Strong coupling in experiments. **a** Open cavity based on two separated DBR mirrors (shaded blue), the ML TMDC (dark gray) is on the bottom mirror<sup>79</sup>. **b** The distance between the mirrors is controlled by a piezo stepper motor, which allows to tune the optical cavity mode into resonance with the TMDC exciton transition, leading to an anticrossing at resonance. **a, b** Reproduced from Dufferwiel et al.<sup>79</sup> **c** Strong light-matter coupling conditions in lithographically defined second order grating structures<sup>82</sup>. The TMDC ML is exfoliated directly onto the silicon nitride structure. **d** The anticrossing between cavity mode predicted by theory (Sim) is clearly observed in the PL measurements (Exp). **c, d** Reproduced from Zhang et al.<sup>82</sup> **e** Hybrid microcavity with DBR at the bottom and thin metal layer on top<sup>85</sup>. **f** The lower and upper polariton branch are observed, with error bars of the energy position given by the lineshape analysis and spectral resolution of the experiment. The position of the cavity resonance C and the exciton resonance X in the absence of coupling are marked by dashed lines. **e, f** Reproduced from Lundt et al.<sup>85</sup>

formation of exciton-polaritons was more recently convincingly demonstrated in a fully monolithic cavity in an intermediate temperature regime between 110 and 230 K<sup>81</sup>. Interestingly, strong light-matter coupling conditions in lithographically defined grating structures with a single WS<sub>2</sub> monolayer have also been established at room temperature. This approach completely bypasses the difficulties related to capping the atomic monolayer for the integration into microcavities<sup>82</sup>, see Fig. 3e and f.

**Strong coupling of MLs in metal-based microcavities.** In order to clearly manifest strong-coupling conditions at room temperature with single MLs, one strategy involves to replace either one, or both of the DBR mirrors by thin metal layers. In appropriate designs comprising a metal-capped DBR layer, this approach can give rise to so-called Tamm plasmon states, which have significantly reduced mode volumes and thus can be expected to yield increased Rabi splitting<sup>83,84</sup>. Strong-coupling conditions with a single monolayer of WSe<sub>2</sub> as well as MoS<sub>2</sub> in such structures have been reported based on angle-resolved studies. Interestingly, in both efforts, the authors succeeded to map out the full dispersion relation of both the upper and lower polariton branch, as well as the characteristic anticrossing of the normal mode of the system<sup>85,86</sup>, see Fig. 3c and d. In order to further reduce the effective cavity length and thus increase the coupling strength, approaches involving purely metal-based Fabry–Perot cavities were reported in refs. <sup>87,88</sup> While these approaches intrinsically suffer from rather low cavity quality factors (typically < 100), the observed Rabi-splittings were very large, on the scale of 100 meV.

**Strong coupling with plasmonic structures.** One route towards further enhancement of the light-matter coupling strength is based on plasmonic resonant structures<sup>89</sup>. They also allow to

develop truly nanophotonic approaches to confine the light field below the optical diffraction limit. Such devices have been shown to be well compatible with the standard exfoliation and transfer technologies commonly applied in TMDC research. Among the various kinds of available structures, two species of devices have been mostly investigated thus far: the first involves a periodic arrangement (lattices) of metallic nanostructures. Such structures can, e.g., consist of a planar metal layer with holes, or an array of metal disks supporting localized surface plasmon resonances. Here, effects of light-matter coupling have been studied<sup>88,90</sup>, and polaritonic behavior was observed. Nevertheless, while the observed coupling strengths were significant, a clearly resolved split doublet of normal modes was mostly screened by strong broadening effects associated by optical losses in the metal structures.

The situation becomes even more delicate for systems comprising a single plasmonic resonator coupled to a monolayer: there, it is no longer possible to study the dispersion relation of quasi-particles via angle-resolved luminescence or reflection spectroscopy due to full mode quantization, and the signal strength in standard reflectivity spectra is low. Therefore, a method of choice to investigate light-matter coupling in such systems is so-called darkfield scattering. Thus far, there are a series of reports investigating strong-coupling conditions in TMDC-nanocavity hybrid systems. This includes a demonstration of a two peaked scattering spectrum from a single silver nanorod and a monolayer of WSe<sub>2</sub><sup>91</sup>, respectively a gold rod and a WS<sub>2</sub> layer<sup>92</sup> and an ultra-compact gold nanogap resonator<sup>93</sup>. Both reports base their claim primarily on the observation of an anticrossing mode doublet in darkfield scattering spectra, which were acquired by studying a variety of nanorod lengths to facilitate tuning of the optical resonance frequency. However, it is important to note, that split-peak spectra acquired in darkfield

scattering measurements in closely related structures have been priorly interpreted in the framework of weak coupling: Here, the observed anticrossing is merely a result of enhanced absorption by the excitonic resonance in the presence of a broad optical resonance<sup>94</sup>. These ongoing developments indicate the need for complementary experimental evidence to better establish the conditions for observation of strong coupling in these systems. Possible experiments include micro-PL measurements or studies in the time domain.

**Polaritons and valley selectivity.** A unique feature in TMDC-based microcavity systems is the possibility to optically address the valley degree of freedom, i.e., optical transitions in distinct valleys in momentum space<sup>66</sup>. Valley polarization of excitons in WS<sub>2</sub>, WSe<sub>2</sub>, and MoS<sub>2</sub> is now routinely observed in high-quality samples even under non-resonant excitation conditions<sup>10,11,95</sup>. In contrast, similar experiments in MoSe<sub>2</sub> MLs only resulted in very low circular polarization of the exciton PL of the order of 5%<sup>96</sup>. The dynamic process of valley polarization and depolarization strongly depends on the carrier redistribution, scattering and emission lifetime, and thus it is reasonable to assume that it can be tailored by coupling the excitonic resonances to microcavity modes.

In order to scrutinize whether the effects of valley polarization become more pronounced in strongly coupled microcavities, a variety of experiments have been designed very recently: in refs. <sup>97,98</sup>, the authors have studied a system composed of a single MoSe<sub>2</sub> monolayer in the strong-coupling regime with a microcavity mode. Both works independently confirmed, that strong-coupling conditions can retain the valley polarization of the excitations in MoSe<sub>2</sub> at cryogenic temperatures, by an amplification of the scattering dynamics. In addition, it was also demonstrated, that the valley index can be directly addressed in the strong-coupling regime by a resonant laser in a Raman-scattering experiment<sup>97</sup>. The great interest to manipulate and enhance spin- and spin-valley-related phenomena in the strong-coupling regime, even up to ambient conditions, is further reflected by a series of papers from different groups, which demonstrated the valley-tagged exciton-polaritons at ambient conditions<sup>99–101</sup> based on MLs of MoS<sub>2</sub> and WS<sub>2</sub>. These results confirm the great potential of strongly coupled systems to play a crucial role in future valleytronic architectures, where the valley index of monolayer excitons can be married with ultra-fast propagation and low power switching inherited by the polariton nature.

**Hybrid polaritonics.** In principle, it is possible to generate hybrid states of various excitonic transitions which are coherently coupled to the same photonic mode. These so-called hybrid polaritons have raised considerable interest recently, as they can provide a pathway to combine the advantages of various material systems in one device<sup>102</sup>. One example, for instance, involves the case of hybrid structures with embedded semiconductor quantum wells and atomic MLs. Here, electric current can be injected into one or multiple semiconductor quantum wells which are embedded in a conventional *p-i-n* heterostructure. This QW-light-emitting diode (LED) can be integrated in the bottom DBR section or into the microcavity. There are two possible processes of coupling between the semiconductor QW and the excitons in the two-dimensional crystals. If coupling between the two excitations is negligible or resonance conditions cannot be established, the semiconductor LED will simply act as an internal light source to excite the excitons in the two-dimensional crystals. However, if strong-coupling conditions can simultaneously be established in the quantum wells and the monolayer crystal with the same photonic resonance, hybrid

polaritons composed of excitons in dielectric quantum wells and MLs can evolve in the system. Such excitations have been observed in ref. <sup>103</sup> based on a microcavity with four embedded GaAs quantum wells and a single monolayer of MoSe<sub>2</sub>.

Light-matter hybridization in the collective strong-coupling regime between monolayer excitons and III–V excitons is also a viable tool to directly influence interactions in the polariton system. It is widely believed, that polariton condensation is strongly facilitated by exciton–exciton exchange interactions, which can yield a stimulated scattering mechanism into a polariton ground state and thus lead to its macroscopic population. This interaction matrix element is given by  $\mathcal{M} = CE_B a_B^2 \sim e^2 a_B / \epsilon_{\text{eff}}$ , where  $E_B \sim e^2 / (\epsilon_{\text{eff}} a_B)$  is the exciton binding energy evaluated in the hydrogenic model with the effective screening constant  $\epsilon_{\text{eff}}$  and  $C$  is a constant.  $\mathcal{M}$  scales with the excitonic Bohr radius<sup>104,105</sup>, which is rather small (on the order of 1 ... 2 nm) in most TMDC materials. Despite somewhat weak dielectric screening in TMDC MLs, exciton–exciton interaction turns out to be less efficient as compared with III–V semiconductors (the expression for  $\mathcal{M}$  can be also recast via the reduced mass  $\mu$  of the electron–hole pair as  $\mathcal{M} \sim \hbar^2 / \mu$ ). Due to larger effective masses in TMDCs, the interactions are weaker here than in III–V semiconductor nanosystems). By admixing the properties of strongly interacting excitons in III–V materials and strongly bound valley excitons in TMDCs, it is reasonable to believe that a good compromise can be found to facilitate stimulated Bose condensation at elevated temperatures in optimized devices<sup>106</sup>.

Hybrid polariton states were furthermore identified in structures involving organic as well as two-dimensional materials embedded in a fully metallic open cavity<sup>107</sup>. Such Frenkel–Wannier polaritons should be extraordinarily stable, and represent one promising candidate to observe Bosonic condensation phenomena at strongly elevated temperatures, similar to recent reports on organic-III–V hybrid excitations<sup>108</sup>.

## Outlook

Studies of strong light-matter coupling in two-dimensional semiconductors demonstrate outstanding progress<sup>109</sup>. By now, the strong coupling has been already demonstrated in a number of systems including TMDC MLs in planar microcavities, hybrid organic–inorganic systems, structures with metallic components.

First, from a fundamental point of view studies of various collective phenomena and nonlinear phenomena, including possible Bose–Einstein condensation and superfluidity of polaritons<sup>19,20</sup> in atomically thin semiconductors are very exciting. Since in these systems a truly two-dimensional limit can be realized for excitons, one may expect realizations of novel and previously unexplored facets of complex collective effects in polaritonic systems.

Second, both from fundamental and practical viewpoints studies of chirality effects for excitons in two-dimensional materials interacting with light are very promising in view of recent predictions of substantial natural optical activity in TMDC MLs stacks<sup>110</sup>. Furthermore, realizations of combined systems with TMDC MLs embedded in chiral cavities open up possibilities of realizing room temperature circularly polarized lasing<sup>111</sup>.

Finally, various applications of strong light-matter coupling for ultra-fast optical switching, photon routing and other optoelectronic devices, and, possibly, even for information processing, will naturally appear in the course of further studies of these promising material systems.

Received: 22 December 2017 Accepted: 31 May 2018

Published online: 12 July 2018



## References

- He, K. et al. Tightly bound excitons in monolayer WSe<sub>2</sub>. *Phys. Rev. Lett.* **113**, 026803 (2014).
- Chernikov, A. et al. Exciton binding energy and nonhydrogenic rydberg series in monolayer WS<sub>2</sub>. *Phys. Rev. Lett.* **113**, 076802 (2014).
- Li, Y. et al. Measurement of the optical dielectric function of monolayer transition-metal dichalcogenides: MoS<sub>2</sub>, MoSe<sub>2</sub>, WS<sub>2</sub>, and WSe<sub>2</sub>. *Phys. Rev. B* **90**, 205422 (2014).
- Poellmann, C. et al. Resonant internal quantum transitions and femtosecond radiative decay of excitons in monolayer WSe<sub>2</sub>. *Nat. Mater.* **14**, 889–893 (2015).
- Robert, C. et al. Exciton radiative lifetime in transition metal dichalcogenide monolayers. *Phys. Rev. B* **93**, 205423 (2016).
- Moody, G. et al. Intrinsic homogeneous linewidth and broadening mechanisms of excitons in monolayer transition metal dichalcogenides. *Nat. Commun.* **6**, 8315 (2015).
- Korn, T., Heydrich, S., Hirmer, M., Schmutzler, J. & Schüller, C. Low-temperature photocarrier dynamics in monolayer MoS<sub>2</sub>. *Appl. Phys. Lett.* **99**, 102109 (2011).
- Cao, T. et al. Valley-selective circular dichroism in MoS<sub>2</sub>. *Nat. Commun.* **3**, 887 (2012).
- Xiao, D., Liu, G.-B., Feng, W., Xu, X. & Yao, W. Coupled spin and valley physics in monolayers of MoS<sub>2</sub> and other group-VI dichalcogenides. *Phys. Rev. Lett.* **108**, 196802 (2012).
- Mak, K. F., He, K., Shan, J. & Heinz, T. F. Control of valley polarization in monolayer MoS<sub>2</sub> by optical helicity. *Nat. Nanotechnol.* **7**, 494–498 (2012).
- Sallen, G. et al. Robust optical emission polarization in MoS<sub>2</sub> monolayers through selective valley excitation. *Phys. Rev. B* **86**, 081301 (2012).
- Zeng, H., Dai, J., Yao, W., Xiao, D. & Cui, X. Valley polarization in MoS<sub>2</sub> monolayers by optical pumping. *Nat. Nanotechnol.* **7**, 490–493 (2012).
- Plechinger, G. et al. Trion fine structure and coupled spin-valley dynamics in monolayer tungsten disulfide. *Nat. Commun.* **7**, 12715 (2016).
- Wang, G. et al. Valley dynamics probed through charged and neutral exciton emission in monolayer WSe<sub>2</sub>. *Phys. Rev. B* **90**, 075413 (2014).
- Yang, L. et al. Long-lived nanosecond spin relaxation and spin coherence of electrons in monolayer MoS<sub>2</sub> and WS<sub>2</sub>. *Nat. Phys.* **11**, 830–834 (2015).
- Geim, A. K. & Grigorieva, I. V. Van der waals heterostructures. *Nature* **499**, 419–425 (2013).
- Withers, F. et al. WSe<sub>2</sub> light-emitting tunneling transistors with enhanced brightness at room temperature. *Nano Lett.* **15**, 8223–8228 (2015).
- Weisbuch, C., Nishioka, M., Ishikawa, A. & Arakawa, Y. Observation of the coupled exciton-photon mode splitting in a semiconductor quantum microcavity. *Phys. Rev. Lett.* **69**, 3314–3317 (1992).
- Kavokin, A., Baumberg, J., Malpuech, G. & Laussy, F. *Microcavities* (Oxford University Press, Oxford, 2011).
- Sanvitto, D. & Timofeev, V. *Exciton Polaritons in Microcavities: New Frontiers* Vol. 172 (Springer Science & Business Media, New York, 2012).
- Kavokin, A., Malpuech, G. & Gil, B. Semiconductor microcavities: towards polariton lasers. *Mater. Res. Soc. Internet J. Nitride Semicond. Res.* **8**, e3 (2003).
- Lundt, N. et al. Monolayered MoSe<sub>2</sub>: a candidate for room temperature polaritonics. *2D Mater.* **4**, 015006 (2016).
- Novoselov, K. S. et al. Electric field effect in atomically thin carbon films. *Science* **306**, 666–669 (2004).
- Novoselov, K. S. et al. Two-dimensional atomic crystals. *Proc. Natl Acad. Sci. USA* **102**, 10451 (2005).
- Mak, K. F., Lee, C., Hone, J., Shan, J. & Heinz, T. F. Atomically thin MoS<sub>2</sub>: a new direct-gap semiconductor. *Phys. Rev. Lett.* **105**, 136805 (2010).
- Splendiani, A. et al. Emerging photoluminescence in monolayer MoS<sub>2</sub>. *Nano Lett.* **10**, 1271–1275 (2010).
- Dickinson, R. G. & Pauling, L. The crystal structure of molybdenite. *J. Am. Chem. Soc.* **45**, 1466–1471 (1923).
- Wilson, J. & Yoffe, A. The transition metal dichalcogenides discussion and interpretation of the observed optical, electrical and structural properties. *Adv. Phys.* **18**, 193–335 (1969).
- Li, T. & Galli, G. Electronic properties of MoS<sub>2</sub> nanoparticles. *J. Phys. Chem. C* **111**, 16192–16196 (2007).
- Kuc, A., Zibouche, N. & Heine, T. Influence of quantum confinement on the electronic structure of the transition metal sulfide TS<sub>2</sub>. *Phys. Rev. B* **83**, 245213 (2011).
- Ramasubramanian, A. Large excitonic effects in monolayers of molybdenum and tungsten dichalcogenides. *Phys. Rev. B* **86**, 115409 (2012).
- Song, Y. & Dery, H. Transport theory of monolayer transition-metal dichalcogenides through symmetry. *Phys. Rev. Lett.* **111**, 026601 (2013).
- Kormanyos, A. et al. k.p theory for two-dimensional transition metal dichalcogenide semiconductors. *2D Mater.* **2**, 022001 (2015).
- Ugeda, M. M. et al. Observation of giant bandgap renormalization and excitonic effects in a monolayer transition metal dichalcogenide semiconductor. *Nat. Mater.* **13**, 1091–1095 (2014).
- Wang, G. et al. Colloquium: excitons in atomically thin transition metal dichalcogenides. *Rev. Mod. Phys.* **90**, 021001 (2018).
- Rytova, N. S. Screened potential of a point charge in a thin film. *Proc. MSU, Phys., Astron.* **3**, 30 (1967).
- Keldysh, L. V. Coulomb interaction in thin semiconductor and semimetal films. *Sov. J. Exp. Theor. Phys. Lett.* **29**, 658 (1979).
- Raja, A. et al. Coulomb engineering of the bandgap and excitons in two-dimensional materials. *Nat. Commun.* **8**, 15251 (2017).
- Stier, A. V., Wilson, N. P., Clark, G., Xu, X. & Crooker, S. A. Probing the influence of dielectric environment on excitons in monolayer WSe<sub>2</sub>: insight from high magnetic fields. *Nano Lett.* **16**, 7054–7060 (2016).
- Jakubczyk, T. et al. Radiatively limited dephasing and exciton dynamics in MoSe<sub>2</sub> monolayers revealed with four-wave mixing microscopy. *Nano Lett.* **16**, 5333–5339 (2016).
- Ivchenko, E. L. *Optical Spectroscopy of Semiconductor Nanostructures*. (Alpha Science, Harrow, 2005).
- Selig, M. et al. Excitonic linewidth and coherence lifetime in monolayer transition metal dichalcogenides. *Nat. Commun.* **7**, 13279 (2016).
- Savona, V., Andreani, L., Schwendemann, P. & Quattropani, A. Quantum well excitons in semiconductor microcavities: unified treatment of weak and strong coupling regimes. *Solid State Commun.* **93**, 733–739 (1995).
- Ye, Z. et al. Probing excitonic dark states in single-layer tungsten disulfide. *Nature* **513**, 214–218 (2014).
- Cadiz, F. et al. Excitonic linewidth approaching the homogeneous limit in MoS<sub>2</sub>-based van der waals heterostructures. *Phys. Rev. X* **7**, 021026 (2017).
- Wierzbowski, J. et al. Direct exciton emission from atomically thin transition metal dichalcogenide heterostructures near the lifetime limit. *Sci. Rep.* **7**, 12383 (2017).
- Ajayi, O. A. et al. Approaching the intrinsic photoluminescence linewidth in transition metal dichalcogenide monolayers. *2D Mater.* **4**, 031011 (2017).
- Dery, H. & Song, Y. Polarization analysis of excitons in monolayer and bilayer transition-metal dichalcogenides. *Phys. Rev. B* **92**, 125431 (2015).
- Echeverry, J. P., Urbaszek, B., Amand, T., Marie, X. & Gerber, I. C. Splitting between bright and dark excitons in transition metal dichalcogenide monolayers. *Phys. Rev. B* **93**, 121107 (2016).
- Zhang, X.-X., You, Y., Zhao, S. Y. F. & Heinz, T. F. Experimental evidence for dark excitons in monolayer WSe<sub>2</sub>. *Phys. Rev. Lett.* **115**, 257403 (2015).
- Arora, A. et al. Excitonic resonances in thin films of WSe<sub>2</sub>: from monolayer to bulk material. *Nanoscale* **7**, 10421–10429 (2015).
- Godde, T. et al. Exciton and trion dynamics in atomically thin MoSe<sub>2</sub> and WSe<sub>2</sub>: effect of localization. *Phys. Rev. B* **94**, 165301 (2016).
- Zhang, X.-X. et al. Magnetic brightening and control of dark excitons in monolayer WSe<sub>2</sub>. *Nat. Nanotechnol.* **12**, 883–888 (2017).
- Molas, M. et al. Brightening of dark excitons in monolayers of semiconducting transition metal dichalcogenides. *2D Mater.* **4**, 021003 (2017).
- Wang, G. et al. In-plane propagation of light in transition metal dichalcogenide monolayers: optical selection rules. *Phys. Rev. Lett.* **119**, 047401 (2017).
- Zhou, Y. et al. Probing dark excitons in atomically thin semiconductors via near-field coupling to surface plasmon polaritons. *Nat. Nanotechnol.* **12**, 856–860 (2017).
- Park, K.-D., Jiang, T., Clark, G., Xu, X. & Raschke, M. B. Radiative control of dark excitons at room temperature by nano-optical antenna-tip purcell effect. *Nat. Nanotechnol.* **13**, 59–64 (2018).
- Mak, K. F. et al. Tightly bound trions in monolayer MoS<sub>2</sub>. *Nat. Mater.* **12**, 207–211 (2013).
- Yu, H., Liu, G., Gong, P., Xu, X. & Yao, W. Bright excitons in monolayer transition metal dichalcogenides: from Dirac cones to Dirac saddle points. *Nat. Commun.* **5**, 3876 (2014).
- Jones, A. M. et al. Excitonic luminescence upconversion in a two-dimensional semiconductor. *Nat. Phys.* **12**, 323–327 (2016).
- Courtade, E. et al. Charged excitons in monolayer WSe<sub>2</sub>: experiment and theory. *Phys. Rev. B* **96**, 085302 (2017).
- You, Y. et al. Observation of biexcitons in monolayer WSe<sub>2</sub>. *Nat. Phys.* **11**, 477–481 (2015).
- Plechinger, G. et al. Identification of excitons, trions and biexcitons in single-layer WS<sub>2</sub>. *Phys. Status Solidi* **9**, 457–461 (2015).
- He, Z. et al. Biexciton formation in bilayer tungsten disulfide. *ACS Nano* **10**, 2176–2183 (2016).
- Baranowski, M. et al. Dark excitons and the elusive valley polarization in transition metal dichalcogenides. *2D Mater.* **4**, 025016 (2017).
- Schaibley, J. R. et al. Valley depolarization dynamics and valley hall effect of excitons in monolayer and bilayer MoS<sub>2</sub>. *Nat. Rev. Mater.* **1**, 16055 (2016).
- Glazov, M. M. et al. Exciton fine structure and spin decoherence in monolayers of transition metal dichalcogenides. *Phys. Rev. B* **89**, 201302 (2014).



68. Yu, T. & Wu, M. W. Valley depolarization due to intervalley and intravalley electron-hole exchange interactions in monolayer MoS<sub>2</sub>. *Phys. Rev. B* **89**, 205303 (2014).
69. Volmer, F. et al. Intervalley dark trion states with spin lifetimes of 150 ns in WSe<sub>2</sub>. *Phys. Rev. B* **95**, 235408 (2017).
70. Rivera, P. et al. Valley-polarized exciton dynamics in a 2d semiconductor heterostructure. *Science* **351**, 688–691 (2016).
71. Dey, P. et al. Gate-controlled spin-valley locking of resident carriers in WSe<sub>2</sub> monolayers. *Phys. Rev. Lett.* **119**, 137401 (2017).
72. Andreani, L. C., Tassone, F. & Bassani, F. Radiative lifetime of free excitons in quantum wells. *Solid State Commun.* **77**, 641–645 (1991).
73. Ivchenko, E. L., Kaliteevski, M. A., Kavokin, A. V. & Nesvizhskii, A. I. Reflection and absorption spectra from microcavities with resonant bragg quantum wells. *J. Opt. Soc. Am. B* **13**, 1061–1068 (1996).
74. Walls, D. F. & Milburn, G. J. *Quantum Optics*, 2nd edn (Springer, Berlin, 2008).
75. Schneider, C. et al. Exciton-polariton trapping and potential landscape engineering. *Rep. Progress. Phys.* **80**, 016503 (2016).
76. Purcell, E. M. Spontaneous emission probabilities at radio frequencies. *Phys. Rev.* **69**, 681 (1946).
77. Glazov, M. M., Ivchenko, E. L., Poddubny, A. N. & Khitrova, G. Purcell factor in small metallic cavities. *Phys. Solid. State* **53**, 1753 (2011).
78. Liu, X. et al. Strong light-matter coupling in two-dimensional atomic crystals. *Nat. Photonics* **9**, 30–34 (2015).
79. Dufferwiel, S. et al. Exciton-polaritons in van der waals heterostructures embedded in tunable microcavities. *Nat. Commun.* **6**, 8579 (2015).
80. Sidler, M. et al. Fermi polaron-polaritons in charge-tunable atomically thin semiconductors. *Nat. Phys.* **13**, 255–261 (2017).
81. Liu, X. et al. Control of coherently coupled exciton polaritons in monolayer tungsten disulphide. *Phys. Rev. Lett.* **119**, 027403 (2017).
82. Zhang, L., Gogna, R., Burg, W., Tutuc, E. & Deng, H. Photonic-crystal exciton-polaritons in monolayer semiconductors. *Nat. Commun.* **9**, 713 (2018).
83. Kaliteevski, M. et al. Tamm plasmon-polaritons: possible electromagnetic states at the interface of a metal and a dielectric bragg mirror. *Phys. Rev. B* **76**, 165415 (2007).
84. Sasin, M. et al. Tamm plasmon polaritons: slow and spatially compact light. *Appl. Phys. Lett.* **92**, 251112 (2008).
85. Lundt, N. et al. Room-temperature Tamm-plasmon exciton-polaritons with a WSe<sub>2</sub> monolayer. *Nat. Commun.* **7**, 13328 (2016).
86. Hu, T. et al. Strong coupling between Tamm plasmon polariton and two dimensional semiconductor excitons. *Appl. Phys. Lett.* **110**, 051101 (2017).
87. Flatten, L. C. et al. Room-temperature exciton-polaritons with two-dimensional WS<sub>2</sub>. *Sci. Rep.* **6**, 33134 (2016).
88. Wang, S. et al. Coherent coupling of WS<sub>2</sub> monolayers with metallic photonic nanostructures at room temperature. *Nano Lett.* **16**, 4368–4374 (2016).
89. Cuadra, J. et al. Observation of tunable charged exciton polaritons in hybrid monolayer ws<sub>2</sub>- plasmonic nanoantenna system. *Nano Lett.* **18**, 1777–1785 (2018).
90. Liu, W. et al. Strong exciton-plasmon coupling in MoS<sub>2</sub>- coupled with plasmonic lattice. *Nano Lett.* **16**, 1262–1269 (2016).
91. Zheng, D. et al. Manipulating coherent plasmon-exciton interaction in a single silver nanorod on monolayer WSe<sub>2</sub>. *Nano Lett.* **17**, 3809–3814 (2017).
92. Wen, J. et al. Room-temperature strong light-matter interaction with active control in single plasmonic nanorod coupled with two-dimensional atomic crystals. *Nano Lett.* **17**, 4689–4697 (2017).
93. Kleemann, M. E. et al. Strong-coupling of WSe<sub>2</sub> in ultra-compact plasmonic nanocavities at room temperature. *Nat. Commun.* **8**, 1296 (2017).
94. Kern, J. et al. Nanoantenna-enhanced light-matter interaction in atomically thin WS<sub>2</sub>. *ACS Photonics* **2**, 1260–1265 (2015).
95. Jones, A. M. et al. Optical generation of excitonic valley coherence in monolayer WSe<sub>2</sub>. *Nat. Nanotechnol.* **8**, 634–638 (2013).
96. Wang, G. et al. Polarization and time-resolved photoluminescence spectroscopy of excitons in MoSe<sub>2</sub> monolayers. *Appl. Phys. Lett.* **106**, 112101 (2015).
97. Lundt, N. et al. Valley polarized relaxation and upconversion luminescence from Tamm-plasmon trion-polaritons with a MoSe<sub>2</sub> monolayer. *2D Mater.* **4**, 025096 (2017).
98. Dufferwiel, S. et al. Valley-addressable polaritons in atomically thin semiconductors. *Nat. Photonics* **11**, 497–501 (2017).
99. Sun, Z. et al. Optical control of room-temperature valley polaritons. *Nat. Photonics* **11**, 491–496 (2017).
100. Chen, Y.-J., Cain, J. D., Stanev, T. K., Dravid, V. P. & Stern, N. P. Valley-polarized exciton-polaritons in a monolayer semiconductor. *Nat. Photonics* **11**, 431–435 (2017).
101. Lundt, N. et al. Observation of macroscopic valley-polarized monolayer exciton-polaritons at room temperature. *Phys. Rev. B* **96**, 241403 (2017).
102. Slootsky, M., Liu, X., Menon, V. M. & Forrest, S. R. Room temperature Frenkel-Wannier-Mott hybridization of degenerate excitons in a strongly coupled microcavity. *Phys. Rev. Lett.* **112**, 076401 (2014).
103. Wurdack, M. et al. Observation of hybrid Tamm-plasmon exciton-polaritons with gas quantum wells and a MoSe<sub>2</sub> monolayer. *Nat. Commun.* **8**, 259 (2017).
104. Shahnazaryan, V., Iorsh, I., Shelykh, I. A. & Kyriienko, O. Exciton-exciton interaction in transition-metal dichalcogenide monolayers. *Phys. Rev. B* **96**, 115409 (2017).
105. Tassone, F. & Yamamoto, Y. Exciton-exciton scattering dynamics in a semiconductor microcavity and stimulated scattering into polaritons. *Phys. Rev. B* **59**, 10830 (1999).
106. Waldherr, M. et al. Observation of bosonic condensation in a hybrid monolayer MoSe<sub>2</sub>-GaAs microcavity. Preprint at <https://arxiv.org/abs/1805.03630> (2018).
107. Flatten, L. C. et al. Electrically tunable organic-inorganic hybrid polaritons with monolayer WS<sub>2</sub>. *Nat. Commun.* **8**, 14097 (2017).
108. Paschos, G. et al. Hybrid organic-inorganic polariton laser. *Sci. Rep.* **7**, 11377 (2017).
109. García de Abajo, F. J. Special issue “2d materials for nanophotonics”. *ACS Photonics* **4**, 2959–2961 (2017).
110. Poshakinskiy, A. V., Kazanov, D. R., Shubina, T. V. & Tarasenko, S. A. Optical activity in chiral stacks of 2d semiconductors. *Nanophotonics* **7**, 753–762 (2018).
111. Demenev, A. A. et al. Circularly polarized lasing in chiral modulated semiconductor microcavity with GaAs quantum wells. *Appl. Phys. Lett.* **109**, 171106 (2016).

## Acknowledgements

C.S. thanks the ERC for support within the project Unlimit2D. M.M.G. is grateful to the Russian Science Foundation (Grant No. 17-12-01265). T.K. gratefully acknowledges financial support by the German science foundation (DFG) via grants KO3612/1-1 and KO3612/3-1. S.H. is grateful for support within the EPSRC “Hybrid Polaritonics” Grant (EP/M025330/1). B.U. thanks ANR 2D-vdW-Spin and ERC Grant No. 306719 for financial support.

## Author contributions

C.S., M.M.G., T.K., S.H., and B.U. drafted the manuscript, wrote, and finalized the work together.

## Additional information

**Competing interests:** The authors declare no competing interests.

**Reprints and permission** information is available online at <http://npg.nature.com/reprintsandpermissions/>

**Publisher's note:** Springer Nature remains neutral with regard to jurisdictional claims in published maps and institutional affiliations.



**Open Access** This article is licensed under a Creative Commons Attribution 4.0 International License, which permits use, sharing, adaptation, distribution and reproduction in any medium or format, as long as you give appropriate credit to the original author(s) and the source, provide a link to the Creative Commons license, and indicate if changes were made. The images or other third party material in this article are included in the article's Creative Commons license, unless indicated otherwise in a credit line to the material. If material is not included in the article's Creative Commons license and your intended use is not permitted by statutory regulation or exceeds the permitted use, you will need to obtain permission directly from the copyright holder. To view a copy of this license, visit <http://creativecommons.org/licenses/by/4.0/>.

© The Author(s) 2018